Group Contribution Lattice Fluid Equation of State for CO_2–Ionic Liquid Systems: An Experimental and Modeling Study

Chengna Dai, Zhigang Lei, Wei Wang, Li Xiao, and Biaohua Chen
State Key Laboratory of Chemical Resource Engineering, Beijing University of Chemical Technology, Beijing 100029, China

DOI 10.1002/aic.14166
Published online June 25, 2013 in Wiley Online Library (wileyonlinelibrary.com)

The group contribution lattice fluid equation of state (GCLF EOS) was first extended to predict the thermodynamic properties for carbon dioxide (CO_2)–ionic liquid (IL) systems. The group interaction parameters of CO_2 with IL groups were obtained by means of correlating the exhaustively collected experimental solubility data at high temperatures (above 278.15 K). New group parameters between CO_2 and IL groups were added into the current parameter matrix. It was verified that GCLF EOS with two kinds of mixing rules could be used for predicting the CO_2 solubility in ILs, and volume expansivity of ILs upon the addition of CO_2, as well as identifying the new structure–property relation. Moreover, it is the first work on the measurement of the solubility of CO_2 in ILs at low temperatures (below 278.15 K), manifesting the applicability of predictive GCLF EOS over a wider temperature range. © 2013 American Institute of Chemical Engineers *AIChE J*, 59: 4399–4412, 2013

Keywords: GCLF EOS, ILs, CO_2 solubility, volume expansivity, structure–property relation, low temperatures

Introduction

Due to their unique advantages such as nonvolatility, high solubility, and "designer solvents", ionic liquids (ILs) have been receiving significant attention in separation processes recently, especially for capturing carbon dioxide (CO_2) from natural gas and postcombustion flue gas.[1,2] In some cases, the separation requirement for CO_2 yield and purity is not so strict that the adsorption process operating above room temperatures suffices. However, in the purification of syngas for Fischer–Tropsch (FT) synthesis and the production of ammonia (NH_3), the CO_2 content in syngas must be decreased down to several ppm level (usually < 20 ppm) before entering the reaction section.[3] For this purpose, the world-famous Rectisol process in which methanol is used as the separating agent for capturing CO_2 operates at temperatures as low as 228 K with high CO_2 solubility. Unfortunately, for capturing CO_2 with ILs, no experimental data on CO_2 solubility below 278 K have been reported by far. Therefore, in this work, we decided to measure the CO_2 solubility at low temperatures down to 228 K in three common ILs as the representatives, i.e., $[BMIM]^+[BF_4]^-$, $[HMIM]^+[BF_4]^+$, and $[HMIM]^+[PF_6]^-$. Although there is a great variety of ILs, it is tedious and time-consuming to determine the CO_2 solubility in all kinds of ILs through experiments. Thus, for a better and thorough understanding on the separation and thermodynamic behaviors of CO_2–IL systems, reliable and applicable predictive models are indispensable.[4–7]

The predictive models for treating the phase equilibria of the systems with ILs include activity coefficient models, equations of state, molecular simulations, neural networks, and so on, among which activity coefficient models and equations of state are commonly used due to the solid thermodynamic foundation and fast calculation speed. However, the activity coefficient models, including regular solution theory (RST),[8] universal quasichemical functional-group activity coefficients (UNIFAC),[4,9–11] and conductor-like screening model for real solvent (COSMO-RS)[12–15] models, are not functions of volume, and also not dependent on pressure. On the other hand, the equations of state, such as nonrandom lattice-fluid equation of state (NLF EOS),[16,17] the series of statistical associating fluid theory (SAFT) EOS[18–28] (e.g., perturbed-chain polar SAFT [PCP-SAFT], soft-SAFT, heterosegmented-SAFT, and SAFT-γ), and group-contribution equation of state (GC EOS),[29] would take into account the dependence of phase volume on pressure for calculating the phase equilibria, which is especially important for estimating volume expansivity. For CO_2–IL systems, Karakatsani et al.[30] used tPC-PSAFT EOS to predict the marginal vapor pressure of pure ILs and the solubility of CO_2, CO, N_2, and CHF_3 in $[BMIM]^+[PF_6]^-$. The results showed good agreement with experimental data. The soft-SAFT EOS[25,26] was used to predict the solubility of CO_2, H_2, and Xe in three imidazolium-based IL families with different anions, i.e. $[RMIM]^+[BF_4]^-$, $[RMIM]^+[PF_6]^-$, and $[RMIM]^+[Tf_2N]^-$ (R = ethyl, butyl, hexyl, and octyl), at

Additional Supporting Information may be found in the online version of this article.

Correspondence concerning this article should be addressed to Z. Lei at leizhg@mail.buct.edu.cn.

© 2013 American Institute of Chemical Engineers

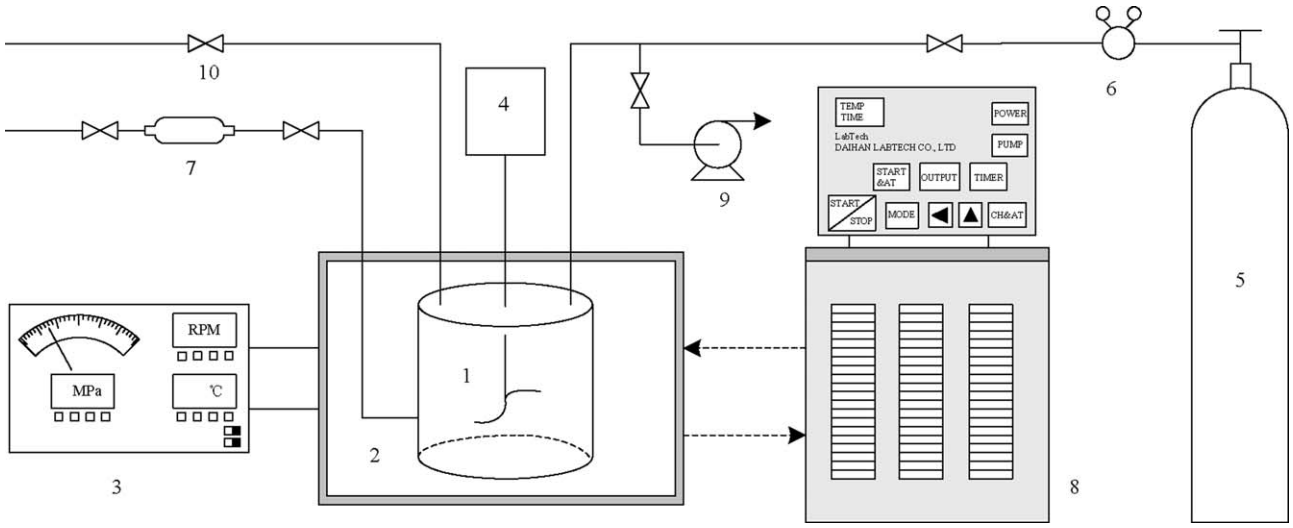

Figure 1. Schematic diagram of the experimental apparatus for measuring the solubility of CO_2 in ILs at low temperatures.

(1) stainless steel autoclave; (2) ethanol bath; (3) pressure and temperature display; (4) stirring paddle; (5) CO_2 cylinder; (6) cylinder regulator (7) liquid sampler; (8) refrigeration compressor; (9) vacuum pump; (10) valve.

pressures up to 100 MPa, and the predicted results were in quantitative agreement with the experimental data. Ji and Adidharma[22,23] compared the experimental data with the predicted results by heterosegmented-SAFT EOS on the solubility of CO_2 in $[RMIM]^+[BF_4]^-$, $[RMIM]^+[PF_6]^-$, and $[RMIM]^+[Tf_2N]^-$ at temperatures up to 423 K and pressures up to 200 bar, and found that both agreed well, especially at low pressures. The ePC-SAFT model[27] introducing a Debye–Hückel Helmholtz energy term improved the prediction of gas solubility in imidazolium-based ILs at temperatures from 293 to 450 K and pressures up to 950 bar. Recently, the SAFT-γ approach[24] was developed to predict the phase behavior of CO_2–IL systems by using the optimized group parameters. Although in most cases the SAFT models could give good predictive results, a number of pure component parameters and cross-association binary parameters have to be concerned, and their equation forms are much complicated. Thus, the simple and reliable group-contribution lattice-fluid equation of state (GCLF EOS), which assumes that the interaction energy between particular groups will be constant regardless of the overall structure of the components, is worth developing for predicting the phase equilibrium of CO_2–IL systems.

GCLF EOS was originally developed by High and Danner.[31,32] Later, Lee and Danner extended it to the polymer–solvent systems.[33] A complete parameter matrix of GCLF EOS for both conventional solvents and polymers has already been established.[34] Afterward, Hamedi et al.[35] extended the predictive model to the solubility prediction of CO_2–polymer binary systems. In our previous work, GCLF EOS was firstly extended to systems containing ILs.[36] However, the prediction of gas (especially CO_2) solubility in ILs by GCLF EOS has not been studied so far.

Therefore, the focus of this work is on addressing the cogently interesting issues for GCLF EOS as to (1) adding the group parameters of CO_2 and ILs groups to the current parameter matrix; (2) checking the applicability of GCLF EOS when extrapolated from high (above 278.15 K) to low temperatures (below 278.15 K); (3) checking the availability in predicting the volume expansivity upon addition of CO_2 into ILs; and (4) identifying the new structure–property relation between molecular structure of ILs and separation performance. For this purpose, the solubility data of CO_2 in $[N_{1,8,8,8}]^+[Tf_2N]^-$, $[N_{1,4,4,4}]^+[Tf_2N]^-$, and $[P_{1,4,4,4}]^+[Tf_2N]^-$ at 298.2 K were measured in this work. The meanings of abbreviations for cations and anions of ILs throughout this article are given in Supporting Information.

Experimental Section

Materials

The ILs $[BMIM]^+[BF_4]^-$, $[HMIM]^+[BF_4]^-$, $[HMIM]^+[PF_6]^-$, $[N_{1,8,8,8}]^+[Tf_2N]^-$, $[N_{1,4,4,4}]^+[Tf_2N]^-$, and $[P_{1,4,4,4}]^+[Tf_2N]^-$ with mass fraction purity > 99 wt % were purchased from Shanghai Chengjie Chemical Co. Before the solubility measurements, the ILs were dried in the vacuum rotary evaporator at 333.2 K for 24 h to remove traces of water and other volatile impurities. The water content in ILs after drying (but before solubility experiments) was less than 400 ppm as determined by Karl Fischer titration (SC-6) in our laboratory, but it became less than 700 ppm after solubility experiments. Thus, the recycled ILs should be dried again to the same water content before further use. A high purity of CO_2 (>99.995 wt %) supplied by Longkou City Gas Plant was used without further purification.

Apparatus and procedure

The solubility of CO_2 in ILs was measured using a low-temperature equilibrium technique, and the apparatus is shown schematically in Figure 1, which mainly consists of a 500 mL stainless steel equilibrium cell, a temperature-controlled ethanol bath producing low temperature down to 213 K in connection with a refrigeration compressor (Model LCC-R220U, made by Daihan Labtech Co.), a stirring paddle, and a liquid sampler.

A certain amount of IL (about 200 mL) was first loaded into the equilibrium cell that was immersed into the ethanol bath for controlling the cooling temperature with a fluctuation of $\pm$ 0.1 K. The temperature was monitored with a thermocouple and a digital thermometer with an uncertainty of 0.1 K. Then

the air in the equilibrium cell was purged out of the system by vacuum pump (2XZ-1). Afterward, a charge of CO_2 was introduced into the equilibrium cell. When CO_2 was dissolved into the IL, the system pressure decreased gradually. The IL phase was mixed with a stirring paddle at a stirring speed of about 200 rpm. It was assumed that gas–liquid equilibrium had been reached until the system pressure measured by a pressure gauge (HQ sensor 1000) with an uncertainty of ± 0.01 MPa was invariable. Generally, the gas–liquid equilibrium took about three days for each data point.

The gas phase was considered as pure CO_2 gas (i.e., $y_1 = 0$) since IL had a negligible vapor pressure,[37] and thus no need to analyze. For each run, a small amount of liquid sample about 2 mL was taken out from the liquid phase. After sampling, the pressure in the equilibrium cell was kept constant with a fluctuation of 0.01 MPa by charging additional CO_2 for next reproducible measurement. Meanwhile, the amounts of CO_2 and IL in the liquid sample were determined using gravimetric method by measuring the weight of solutions with and without CO_2 in the similar way as reported in previous publication.[38] The mass uncertainty of the electronic balance (CPA 1003S, Sartorius) was 0.001 g. Therefore, the estimated uncertainty of solubility measurement in mole fractions was less than 0.006. For each data point, three runs were performed to check the reproducibility of the results at the same temperature and pressure, and to ensure that no degradation of IL took place. The reliability of experimental apparatus and procedure was validated by comparing the obtained experimental solubility data of CO_2 at 298.2 K in $[BMIM]^+[BF_4]^-$ and $[HMIM]^+[BF_4]^-$ with the results reported in different references,[16,39–43] and it was found that the ARDs (average relative deviations) were 2.29% for $[BMIM]^+[BF_4]^-$ (Ref. 40) and 1.82% for $[HMIM]^+[BF_4]^-$ (Ref. 16), respectively (see Supporting Information for detailed values).

Thermodynamic Model

Model description

In this work, ILs were divided into several separate functional groups, and the skeleton of cation and anion was treated as a whole functional group as the same manner as in the UNIFAC model and other group-contribution equations of state for ILs.[4,16,36,44,45] Thus, the additional Debye–Hückel term accounting for long-range (LR) electrostatic contributions can be avoided.

In the GCLF EOS, each molecule or group is assumed to occupy a number of lattice sites, and each lattice site is assumed to have a constant volume ($v_h = 9.75 \times 10^{-3} \cdot m^3 \cdot kmol^{-1}$) with a fixed coordination number ($z = 10$) as commonly used.[31–36] The equation form of GCLF EOS is written as

$$\frac{\tilde{P}}{\tilde{T}} = \ln\left(\frac{\tilde{v}}{\tilde{v}-1}\right) + \frac{z}{2}\ln\left(\frac{\tilde{v}+q}{r-1\tilde{v}}\right) - \frac{\theta^2}{\tilde{T}} \tag{1}$$

where $\tilde{P}$, $\tilde{T}$, and $\tilde{v}$ are the reduced pressure, temperature, and molar volume, respectively, and expressed as

$$\tilde{P} = \frac{P}{P^*} = \frac{2Pv_h}{z\varepsilon^*}, \quad \tilde{T} = \frac{T}{T^*} = \frac{2RT}{z\varepsilon^*}, \quad \tilde{v} = \frac{v}{v^*} = v_h r \tag{2}$$

$$\theta = \frac{q/r}{\tilde{v}+q/r-1}, \quad zq = (z-2)r+2 \tag{3}$$

where q is the interaction surface area parameter; r is the number of lattice sites occupied by a molecule or a group; and R is the universal gas constant (8.314 $J \cdot mol^{-1}$). The adjustable parameters contain the molecular interaction energy ε^* and molecular reference volume v^*.

For a pure component, GCLF EOS contains only two adjustable parameters, $\varepsilon^*$and v^*, as mentioned above. Once the two parameters are known, all of the remaining parameters in Eq. 1 can be determined from Eqs. 2 and 3 at a given temperature and pressure, and then the properties of a system can be obtained according to Eq. 1 with respect to reduced volume. ε^* and v^* are obtained from the following mixing rule

$$\varepsilon_i^* = \sum_k \sum_m \Theta_k^{(i)} \Theta_m^{(i)} (e_{kk} e_{mm})^{1/2} \tag{4}$$

$$v_i^* = \sum_k n_k^{(i)} R_k \tag{5}$$

where e_{kk} is the group interaction energy between like groups k; $\Theta_k^{(i)}$ is the surface area fraction of group k in pure component i; R_k is the group reference volume; and $n_k^{(i)}$ is the number of group k in pure component i

$$e_{kk} = e_{0,k} + e_{1,k}\left(\frac{T}{T_0}\right) + e_{2,k}\left(\frac{T}{T_0}\right)^2 \tag{6}$$

$$\Theta_k^{(i)} = \frac{n_k^{(i)} Q_k}{\sum_n n_n^{(i)} Q_n} \tag{7}$$

$$R_k = \frac{1}{10^3}\left[R_{0,k} + R_{1,k}\left(\frac{T}{T_0}\right) + R_{2,k}\left(\frac{T}{T_0}\right)^2\right] \tag{8}$$

where $e_{i,k}$ and $R_{i,k}$ are constants; T (K) is the system temperature; T_0 is arbitrarily set to 273.15 K; and Q_k is the dimensionless surface area parameter of group k, as used in the UNIFAC model.

The densities of most of pure ILs vary from 0.9 to 1.7 $g \cdot cm^{-3}$, which are not very sensitive to temperature change.[46] Therefore, for IL groups, it is reasonable to assume that $e_{1,k} = e_{2,k} = 0$ and $R_{1,k} = R_{2,k} = 0$.

For a binary mixture, GCLF EOS also requires one binary interaction parameter k_{12}. The solving procedure is similar to that of pure components, but the following mixing rules are introduced

$$\varepsilon_i^* = \bar{\theta}_1 \varepsilon_{11} + \bar{\theta}_2 \varepsilon_{22} - \bar{\theta}_1 \bar{\theta}_2 \dot{\Gamma}_{12} \Delta\varepsilon, \Delta\varepsilon = \varepsilon_{11} + \varepsilon_{22} - 2\varepsilon_{12} \tag{9}$$

$$\varepsilon_{12} = (\varepsilon_{11}\varepsilon_{22})^{1/2}(1-k_{12}), \varepsilon_{ii} = \sum_k \sum_m \Theta_k^{(i)} \Theta_m^{(i)} (e_{kk} e_{mm})^{1/2} \tag{10}$$

$$v^* = \sum_i x_i v_i^* \tag{11}$$

where $\dot{\Gamma}_{12}$ is the nonrandomness parameter between molecules 1 and 2. The quasichemical approach gives the following relationship among the nonrandomness parameters

$$\frac{\dot{\Gamma}_{11}\dot{\Gamma}_{22}}{\dot{\Gamma}_{12}^2} = \exp\left(\theta\frac{\Delta\varepsilon}{RT}\right) \tag{12}$$

Table 1. Group Binary Interaction Parameters ($\alpha_{12}=\alpha_{21}$) Between CO_2 (1) and IL (2) Groups for Mixing Rules MR1 and MR2

	α_{12}	
Main Groups	MR1	MR2
[MIM][BF_4]	−0.3440	−0.0319
[MIM][Tf_2N]	−0.5956	−0.1728
[MIM][PF_6]	−0.3840	−0.0476
[MIM][TfO]	−0.5329	−0.1328
[MIM][$MeSO_4$]	−0.2314	−0.0724
[MIM][$EtSO_4$]	−0.3261	−0.0877
[MIM][Cl]	−0.1933	0.0348
[MIM][$DEPO_4$]	−0.4051	−0.0939
[MIM][$DMPO_4$]	−0.2260	−0.0506
[MIM][$MDEGSO_4$]	−0.4063	−0.0961
[MIM][NO_3]	−0.4810	−0.0468
[MIM][SCN]	−0.4287	−0.1164
[MIM][TFA]	−0.4349	−0.0881
[OCH_2MIM][Tf_2N]	−3.2192	−0.7049
[MPY][BF_4]	−0.4105	−0.0080
[MPY][Tf_2N]	−0.6032	−0.1677
[MPYR][Tf_2N]	−0.5734	−0.1527
[MPYR][TfO]	−0.4762	−0.0849
[N][Tf_2N]	−0.9433	−0.1228
[P][Tf_2N]	0.2771	−0.3216
[P][Cl]	10.6343	−0.2728
[P][TOS]	1.6997	0.3688

The interaction parameter k_{12} can be calculated by two kinds of mixing rules, namely as MR1 and MR2, expressed as

$$k_{12}=\sum_m \sum_n \Theta_m^{(\mathrm{M})}\Theta_n^{(\mathrm{M})}\alpha_{mn} \tag{13}$$

$$\Theta_k^{(\mathrm{M})}=\frac{\sum_i n_k^{(i)}Q_k}{\sum_p \sum_i n_p^{(i)}Q_p} \tag{14}$$

where $\Theta_k^{(\mathrm{M})}$ is the surface area fraction of group k in the mixture containing all groups; and α_{mn} is the group binary interaction parameter. MR1 is expressed in such a way that the interaction parameter is obtained as a correction for the interaction of same and different species. However, for CO_2–polymer systems, Hamedi et al.[35] proposed an alternative formulation (MR2) in which the interaction parameter was calculated only as a contribution of groups from different species

$$k_{12}=\sum_m \sum_n \Theta_m^{(1)}\Theta_n^{(2)}\alpha_{mn}\ (\mathrm{MR2}) \tag{15}$$

$$\Theta_k^{(i)}=\frac{n_k^i Q_k}{\sum_p n_p^{(i)}Q_p} \tag{16}$$

where $\Theta_k^{(i)}$ is the surface area fraction of group k in pure component i.

Other parameters for a binary mixture are calculated from the following equations

$$r=\sum x_i r_i,\quad q=\sum x_i q_i,\quad \theta=\sum x_i \theta_i \tag{17}$$

$$r_i=\frac{v_i^*}{v_{\mathrm{h}}},\quad zq_i=(z-2)r_i+2 \tag{18}$$

$$\theta_i=\frac{q_i/r_i}{\tilde{v}_i/r_i-r_i+q_i},\quad \bar{\theta}_i=\frac{x_i q_i}{q} \tag{19}$$

$$\bar{\theta}_1\dot{\Gamma}_{11}+\bar{\theta}_2\dot{\Gamma}_{12}=\bar{\theta}_2\dot{\Gamma}_{22}+\bar{\theta}_1\dot{\Gamma}_{12}=1 \tag{20}$$

In GCLF EOS, mole fraction activity coefficient (MFAC) of component i in the mixture is given as follows

$$\ln\gamma_i=\ln\frac{a_i}{x_i}=\ln\varphi_i-\ln\ x_i+\ln\tilde{v}_i\tilde{v}+q_i\ln\left(\frac{\tilde{v}}{\tilde{v}-1}\frac{\tilde{v}_i-1}{\tilde{v}_i}\right)+q_i\left(\frac{2\theta_{i,p}-\theta}{\tilde{T}_i}-\theta\tilde{T}\right)+\frac{zq_i}{2}\ln\dot{\Gamma}_i \tag{21}$$

$$\varphi_i=\frac{x_i v_i^*}{\sum_j x_j v_j^*}=\frac{x_i r_i}{\sum_j x_j r_j} \tag{22}$$

where the subscript i represents a pure component i; x_i is the mole fraction of component i in the liquid phase; $\dot{\Gamma}_i$ is nonrandomness parameter; φ_i is the volume fraction of component i in the mixture; and $\theta_{i,p}$ is the surface area fraction of pure component i at the same temperature and pressure as in the mixture.

The group parameters ($e_{0,k}$, $R_{0,k}$, Q_k) for IL groups, and ($e_{0,k}$, $e_{1,k}$, $e_{2,k}$, $R_{0,k}$, $R_{1,k}$, $R_{2,k}$, Q_k) for CO_2 and other groups have been reported in previous references.[34–36,47–49] Therefore, the group binary interaction parameters (α_{mn}) between CO_2 and IL groups are the only required input parameters for solving the above equations, which were derived by means of correlating the experimental solubility data.

Procedure of the estimation of group interaction parameters

The following minimized objective function (OF) was used to obtain the group binary interaction parameters α_{mn} between CO_2 and IL groups

$$\mathrm{OF}=\sum_{i=1}^{N}\left|\frac{x_{i,IL}(\mathrm{GCLF\quad EOS})-x_{i,IL}(\mathrm{exp.})}{x_{i,IL}(\mathrm{exp.})}\right| \tag{23}$$

where N is the number of data points; $x_{i,\mathrm{IL}}$ (exp.) is the experimental solubility of CO_2 in ILs exhaustively collected from references by the end of December 2012; and $x_{i,\mathrm{IL}}$ (GCLF EOS) is the predicted result by GCLF EOS. The kinds of ILs, more than 5300 data points, experimental methods, and the corresponding cited references are provided in detail in Supporting Information. It should be noted that all experimental temperatures reported in the references were above 278.15 K. The SOLVER function with the optimization algorithm of Newton's central difference in Microsoft Excel 2003 was used to correlate α_{mn} to minimize the objective function. In this way, we can clearly deal with so many experimental data collected from references. As a result, the obtained group binary interaction parameters α_{mn} between CO_2 and 22 IL groups using mixing rules MR1 and MR2 are listed in Table 1. The current GCLF EOS parameter matrix is also illustrated in Figure 2. It should be mentioned that the group binary interaction parameters which are available in previous references remain constant.

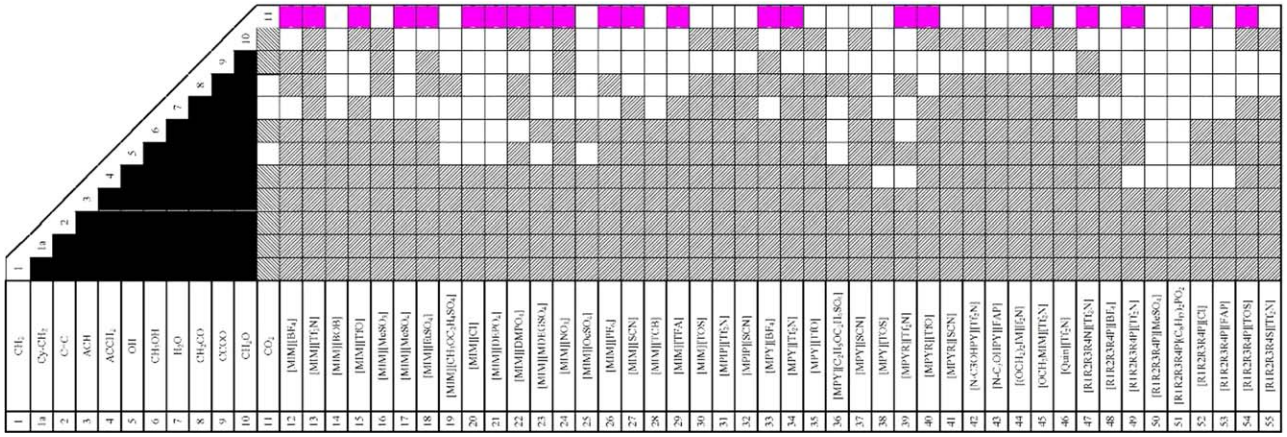

Figure 2. Current GCLF EOS parameter matrix for IL groups.

■ Previously published parameters[47]; ▧ Previously published parameters[48]; ▨ Previously published parameters[36]; ■ New parameters; □ No parameters available. [Color figure can be viewed in the online issue, which is available at wileyonlinelibrary.com.]

Results and Discussion

Prediction of solubility of CO_2 in ILs at high temperatures

The solubility data of CO_2 in 45 kinds of ILs were investigated at temperatures of 278–453 K and at pressures of 0.01–971.00 bar, and the comparison of experimental solubility of CO_2 in ILs with the predicted results (MR1 and MR2) by GCLF EOS is summarized in Table 2, where the ARD is defined as

$$\text{ARD}\,(\%)=\frac{1}{N}\sum_{i=1}^{N}\left|\frac{x_{i,IL}(\text{cal.})-x_{i,IL}(\text{exp.})}{x_{i,IL}(\text{exp.})}\right|\times 100 \qquad (24)$$

The predicted CO_2 solubility data in five common ILs, i.e., $[BMIM]^+[BF_4]^-$, $[BMIM]^+[PF_6]^-$, $[BMIM]^+[Tf_2N]^-$, $[BMPYR]^+[Tf_2N]^-$, and $[BPY]^+[BF_4]^-$, are exemplified in Figure 3, along with the experimental results obtained from references. They exhibit the similar trend and agree very well. The extensive experimental data and the predicted results by GCLF EOS with mixing rules MR1 and MR2, as well as those by the COSMO-RS (conductor-like screening model for real solvents) model using the commercial ADF software,[104] are given in the form of MS Excel spreadsheet in Supporting Information. The comparison shows that GCLF EOS gives better prediction than COSMO-RS model in most cases, and the predicted results by GCLF EOS with both MR1 and MR2 mixing rules are in good agreement with the experimental data.

On the other hand, other equations of state have also been proposed for predicting the solubility of CO_2 in ILs. Ashrafmansouri and Raeissi[24] used the SAFT-γ model involving a number of binary interaction parameters (two parameters accounting for the association between CO_2 and anion, two temperature-independent parameters between CO_2 and CH_3 or CH_2 groups, and two temperature-dependent parameters between CO_2 and anion) to predict the solubility of CO_2 in imidazolium-based ILs. The ARDs for $[BMIM]^+[Tf_2N]^-$ and $[HMIM]^+[Tf_2N]^-$ in their work are 2.33% and 4.04%, respectively, while in this work the corresponding ARDs (MR1) are 4.60% (5.26% for MR2) and 5.20% (7.07% for MR2), respectively. Ji et al.[27] investigated the density of ILs and gas solubility in imidazolium-based ILs using ePC-SAFT, in which the IL was considered to be completely dissociated into a cation and an anion, and five parameters for each ion were required. The introduction of Debye–Hückel Helmholtz energy term shows the best performance, with the result that the ARDs of CO_2 solubility in $[BMIM]^+[Tf_2N]^-$ and $[EMIM]^+[Tf_2N]^-$ are 8.10% and 7.60%, respectively, while in this work the corresponding ARDs are 8.50% (8.62% for MR2) and 9.93% (12.28% for MR2), respectively. This demonstrates that the prediction accuracy of GCLF EOS is comparable with other equations of state which require more model parameters. Therefore, GCLF EOS is applicable for predicting the solubility of CO_2 in ILs at high temperatures.

Prediction of solubility of CO_2 in ILs at low temperatures

The solubility data of CO_2 in $[BMIM]^+[BF_4]^-$, $[HMIM]^+[BF_4]^-$, and $[HMIM]^+[PF_6]^-$ were measured at temperatures (228–273) K and pressures up to 3.0 MPa by means of a low-temperature equilibrium technique. The experimental results are illustrated in Figures 4–6, along with the predicted results by GCLF EOS in which the group binary interaction parameters listed in Table 1 are extrapolated from high to low temperatures. It can be seen that low temperature is favorable for increasing the solubility of CO_2 in ILs significantly. In practice, a high CO_2 solubility at low temperatures can counteract the viscosity increase of pure IL in the mixture. Moreover, the *P–T* diagrams at constant CO_2 composition in three kinds of ILs ($[BMIM]^+[BF_4]^-$, $[HMIM]^+[BF_4]^+$, and $[HMIM]^+[PF_6]^-$) are plotted in Supporting Information including both low- and high-temperature data, and a "continuation" of CO_2 solubility from high to low temperatures is observed.

In summary, the predicted and experimental results are in good agreement. For the GCLF EOS with mixing rule MR1, the ARDs of CO_2 solubility are 5.98, 6.81, and 12.40% for $[BMIM]^+[BF_4]^-$, $[HMIM]^+[BF_4]^-$, and $[HMIM]^+[PF_6]^-$, respectively, while for the GCLF EOS with mixing rule MR2, they are 6.85, 9.76, and 8.70%, respectively. See Supporting Information for more details. Therefore, the application of GCLF EOS can be extended from high to low temperatures. However, it is worth mentioning that the

Table 2. Comparison of Experimental CO_2 Solubility in ILs with the Predicted Results by GCLF EOS

ILs	*T* range (K)	*P* range (bar)	MR1 ARD (%)	MR2 ARD (%)	Number of Data Points	References
$[BMIM]^+[BF_4]^-$	303.72–344.49	0.18–0.84	27.70	25.10	21	[50]
	298.20–333.30	12.09–85.00	15.43	16.48	20	[40]
	283.15–323.15	0.02–13.00	14.38	12.25	84	[41]
	278.47–368.22	5.87–676.20	17.18	18.08	104	[51]
	282.75–348.15	0.10–20.00	18.00	16.59	36	[39]
	303.93–344.27	0.22–0.92	35.24	32.93	11	[52]
	307.55–322.15	17.50–90.00	10.23	12.74	40	[53]
	298.00–298.20	0.10–20.00	23.84	21.61	9	[42]
	293.25–383.15	10.50–246.00	18.39	21.35	59	[54]
	298.15–298.15	6.50–60.70	10.17	10.17	7	[43]
		total ARD	17.14	17.29	391	
$[BMIM]^+[Cl]^-$	353.15–373.15	24.54–369.46	18.36	18.36	45	[55]
$[BMIM]^+[MDEGSO_4]^-$	313.31–333.36	14.30–91.20	32.26	37.45	11	[56]
$[BMIM]^+[MeSO_4]^-$	293.20–413.10	9.08–98.05	11.96	11.83	54	[57]
$[BMIM]^+[NO_3]^-$	313.15–333.15	15.47–93.17	23.96	23.96	21	[58]
	298.20–333.20	10.31–88.92	6.78	6.78	17	[40]
	293.13–368.24	3.68–128.32	14.49	14.49	66	[59]
		total ARD	15.14	15.14	104	
$[BMIM]^+[PF_6]^-$	313.15–323.15	15.17–95.67	14.09	14.05	21	[58]
	283.15–323.15	0.03–12.99	5.72	5.71	158	[60]
	293.15–393.15	1.05–96.85	17.84	17.88	43	[61]
	298.20–333.40	5.60–146.39	9.85	9.85	70	[40]
	283.15–323.15	0.03–13.00	5.40	5.39	158	[41]
	293.29–363.54	4.30–735.00	18.76	18.78	99	[62]
	282.05–348.25	0.10–20.00	12.02	12.01	35	[39]
	297.56–322.52	7.90–80.80	7.34	7.34	42	[63]
	298.15–298.15	5.29–6.67	14.36	14.30	4	[16]
	283.15–343.04	0.41–0.92	36.53	36.50	14	[64]
	298.00–298.20	0.11–20.00	14.84	14.79	9	[42]
	298.15–298.15	2.60–40.20	10.86	10.80	9	[17]
		total ARD	10.42	10.41	662	
$[BMIM]^+[SCN]^-$	292.35–384.15	10.50–315.00	7.24	7.24	56	[54]
$[BMIM]^+[Tf_2N]^-$	298.10–333.30	11.38–132.43	2.68	3.05	55	[40]
	283.15–323.15	0.01–13.00	13.53	13.58	96	[41]
	279.98–339.97	2.92–48.00	7.28	7.57	16	[65]
	283.36–343.78	0.68–1.12	15.45	14.35	14	[66]
	293.35–344.55	10.70–428.00	11.02	9.91	84	[67]
	313.15–453.15	4.20–142.61	7.47	8.78	133	[68]
	292.65–363.26	6.29–499.90	12.75	11.89	68	[69]
	313.20–323.20	80.80–199.40	5.76	5.35	8	[70]
		total ARD	9.73	9.80	474	
$[BMIM]^+[TFA]^-$	298.17–333.41	11.70–92.60	9.69	5.82	19	[56]
	298.00–298.20	0.11–20.00	33.77	20.54	9	[42]
	293.25–363.18	9.79–629.89	21.75	19.35	52	[71]
		total ARD	20.24	16.27	80	
$[BMIM]^+[TfO]^-$	298.20–333.30	10.44–114.77	10.42	13.46	27	[40]
	303.85–344.55	8.50–375.00	19.84	16.69	65	[72]
	303.20–343.20	2.15–65.21	20.50	27.14	35	[73]
		total ARD	18.02	18.88	127	
$[BMPYR]^+[Tf_2N]^-$	283.15–323.15	0.02–13.00	23.27	27.74	52	[41]
	303.78–344.15	0.49–0.57	47.22	44.85	11	[74]
	293.10–413.20	2.80–108.13	4.30	4.66	26	[75]
	303.15–373.15	6.80–627.70	12.61	12.09	72	[76]
	313.20–323.20	80.60–200.60	9.18	9.10	8	[70]
		total ARD	16.70	17.75	169	
$[BMPYR]^+[TfO]^-$	303.15–373.25	18.80–702.00	19.18	19.18	64	[77]
$[BPY]^+[BF_4]^-$	313.15–333.15	15.47–95.80	3.24	3.24	21	[58]
$[C_2OMIM]^+[Tf_2N]^-$	303.15–323.15	0.10–1.60	23.58	23.58	18	[78]
$[C_5MIM]^+[Tf_2N]^-$	293.30–363.29	6.18–598.05	10.00	10.00	144	[79]
$[DMIM]^+[Tf_2N]^-$	298.15–343.15	14.74–145.96	4.52	11.31	22	[80]
	298.15–343.15	14.74–145.96	4.52	11.31	22	[81]
	313.15–313.15	20.00–144.00	15.68	21.17	14	[82]
	313.20–323.20	80.70–201.50	9.81	14.59	8	[70]
		total ARD	7.53	13.80	66	
$[EMIM]^+[BF_4]^-$	298.15–298.15	2.51–8.75	26.88	5.19	9	[16]
	303.20–343.20	4.97–43.29	88.77	65.00	25	[83]
	298.20–313.20	5.30–40.60	50.50	29.79	17	[38]
		total ARD	65.09	42.71	51	
$[EMIM]^+[DEPO_4]^-$	313.15–333.15	0.24–1.99	4.44	4.44	22	[84]
$[EMIM]^+[EtSO_4]^-$	313.15–333.15	14.36–94.61	13.92	13.92	21	[58]
	303.20–343.20	2.11–49.62	14.28	14.28	35	[73]
	303.15–353.15	1.22–15.47	3.90	3.90	39	[85]
		total ARD	9.94	9.94	95	
$[EMIM]^+[MDEGSO_4]^-$	303.20–343.20	8.54–67.10	5.38	5.38	30	[86]
$[EMIM]^+[PF_6]^-$	308.14–366.03	14.90–971.00	41.54	36.88	74	[87]
$[EMIM]^+[Tf_2N]^-$	298.15–298.15	2.13–9.03	6.43	14.90	8	[16]
	303.63–344.23	0.43–0.57	49.88	46.22	14	[88]
	283.43–343.07	0.65–0.86	22.60	16.40	5	[66]
	303.63–344.23	0.43–0.57	49.88	46.22	14	[74]

Table 2. *Continued*

ILs	*T* range (K)	*P* range (bar)	MR1 ARD (%)	MR2 ARD (%)	Number of Data Points	References
	312.10–453.15	6.26–147.70	10.84	15.16	191	[89]
	292.75–344.55	12.20–432.00	10.26	12.02	78	[67]
	297.90–298.20	0.50–20.00	5.19	7.62	9	[42]
	292.16–363.55	6.20–478.50	8.65	8.84	153	[79]
	298.15–343.15	12.35–147.94	2.47	3.20	21	[80]
	298.15–343.15	12.35–147.94	2.47	3.20	21	[81]
		total ARD	11.49	13.39	514	
$[EMIM]^+[TFA]^-$	298.10–298.10	0.10–20.00	10.36	10.15	9	[42]
	298.10–348.20	0.10–20.00	19.89	19.29	27	[90]
		total ARD	17.51	17.01	36	
$[EMIM]^+[TfO]^-$	303.85–344.55	8.00–378.00	12.46	12.54	55	[72]
	303.20–343.20	1.80–58.84	30.18	27.00	30	[91]
		total ARD	18.71	17.64	85	
$[HMIM]^+[BF_4]^-$	293.18–368.16	5.40–866.00	20.56	18.99	104	[92]
	298.15–298.15	3.12–8.99	36.67	30.01	8	[16]
	307.55–322.15	21.30–86.40	7.05	4.55	53	[53]
		total ARD	17.00	14.89	165	
$[HMIM]^+[PF_6]^-$	298.31–363.58	6.40–946.00	20.12	19.79	98	[93]
	298.15–298.15	2.96–9.27	20.72	14.93	14	[16]
		total ARD	20.20	19.18	112	
$[HMIM]^+[Tf_2N]^-$	298.10–333.30	13.15–115.58	3.96	4.73	28	[40]
	298.15–298.15	1.64–8.59	17.15	23.36	9	[16]
	293.15–413.20	6.01–99.11	4.14	2.81	25	[94]
	283.16–323.17	0.01–13.00	13.11	14.10	57	[56]
	288.48–343.20	0.29–0.94	42.71	46.92	11	[95]
	281.90–348.60	0.09–19.76	12.97	15.94	72	[96]
	298.15–298.15	1.57–8.40	4.55	7.12	10	[97]
	303.85–344.55	14.00–390.00	10.55	13.10	90	[67]
	297.30–297.40	0.09–19.75	16.18	22.09	10	[42]
	298.15–343.15	8.00–247.08	8.94	9.64	36	[80]
	298.15–343.15	17.93–247.08	9.21	9.86	25	[81]
	278.12–368.44	4.22–143.37	5.92	6.90	123	[98]
		total ARD	9.99	11.68	496	
$[HMIM]^+[TfO]^-$	313.23–313.39	14.94–84.23	19.42	12.50	6	[99]
	303.85–344.55	12.50–363.00	20.47	15.46	70	[72]
		total ARD	20.39	15.23	76	
$[HMMIM]^+[Tf_2N]^-$	298.20–333.30	14.97–118.04	10.46	5.67	29	[40]
$[HMPY]^+[Tf_2N]^-$	283.18–323.15	0.01–13.00	17.88	18.16	56	[56]
$[HMPYR]^+[Tf_2N]^-$	303.15–373.15	10.60–475.50	10.13	10.21	64	[100]
$[MMIM]^+[DMPO_4]^-$	313.15–333.15	0.49–1.75	6.83	6.83	12	[84]
$[N_{1,8,8,8}]^+[Tf_2N]^-$	313.20–323.20	80.80–205.60	6.87	13.16	8	[70]
$[N_{2,1,1,3}]^+[Tf_2N]^-$	313.22–313.25	11.34–94.66	2.69	3.19	8	[99]
$[N_{4,1,1,1}]^+[Tf_2N]^-$	333.23–333.23	15.60–80.90	7.26	5.77	6	[56]
	282.93–343.07	0.36–0.89	44.66	46.37	12	[66]
	313.20–323.20	85.80–196.30	11.36	12.44	8	[70]
		total ARD	17.06	13.81	153	
$[N_{4,4,4,1}]^+[Tf_2N]^-$	298.15–298.15	0.05–5.50	19.29	15.18	11	[41]
$[NMIM]^+[PF_6]^-$	293.15–298.15	8.60–35.40	25.83	21.12	11	[17]
$[OMIM]^+[BF_4]^-$	313.15–333.15	15.61–93.73	12.87	8.16	21	[58]
	307.79–363.29	5.71–858.00	20.33	17.73	100	[101]
	307.55–322.15	41.70–87.20	9.59	5.28	32	[53]
		total ARD	17.06	13.81	153	
$[OMIM]^+[PF_6]^-$	313.15–333.15	16.00–92.88	18.00	14.58	21	[58]
$[OMIM]^+[Tf_2N]^-$	298.20–333.30	13.26–114.69	3.16	7.60	22	[40]
	297.55–344.55	6.80–348.00	17.78	21.65	97	[67]
	303.15–353.15	1.12–20.63	27.90	33.32	43	[102]
		total ARD	18.48	22.84	162	
$[OMIM]^+[TfO]^-$	303.85–344.55	6.80–340.00	20.35	16.06	65	[67]
$[OMPYR]^+[Tf_2N]^-$	303.15–373.15	5.10–359.20	15.30	17.46	72	[100]
$[P_{1,4,4,4}]^+[TOS]^-$	323.15–323.15	0.0034–13.00	6.49	5.25	33	[41]
$[P_{6,6,6,14}]^+[Cl]^-$	302.55–363.68	1.68–245.70	13.97	13.97	69	[103]
	313.20–323.20	82.10–207.10	6.17	6.17	8	[70]
		total ARD	13.16	13.16	77	
$[P_{6,6,6,14}]^+[Tf_2N]^-$	292.88–363.53	1.06–721.85	11.64	11.64	120	[103]
	293.35–375.35	5.30–222.00	9.78	9.78	91	[77]
	313.20–323.20	80.90–201.70	3.90	3.90	8	[70]
		total ARD	15.18	15.18	219	

predicted results by GCLF EOS sometimes do not match the trend of experimental data at low temperatures and high pressures because in this case the equilibrium state is in the vicinity of critical point of CO_2.

Prediction of volume expansivity of ILs

The addition of CO_2 into ILs as well as conventional organic solvents will lead to an increase of the liquid volume. Volume expansivity is an important physical quantity in determining the liquid volume flow rate along the absorption column so as to avoid liquid flooding occurring in the tray or packing. Besides, volume expansivity with high accuracy is also needed in the solubility measurement using a commercial gravimetric microbalance in which buoyancy effect has to be considered. Otherwise, erroneous or even negative solubility data may arise.[60,105] Badilla and

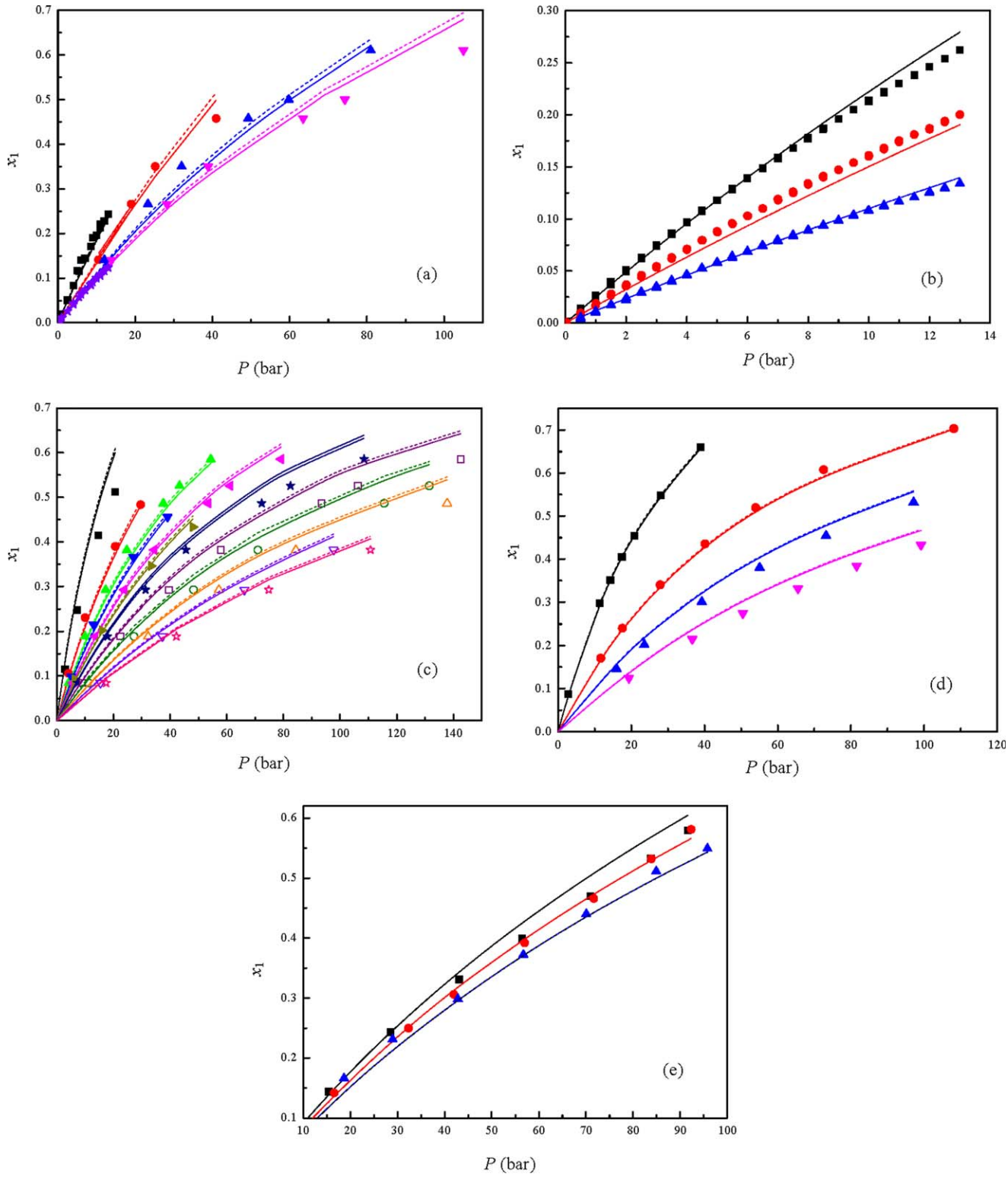

Figure 3. Solubility of CO_2 (1) in five common ILs (2) at various temperatures and pressures.

Solid lines, predicted results by GCLF EOS with MR1; Dashed lines, predicted results by GCLF EOS with MR2; Scattered points, experimental data from references. (a) $[BMIM]^+[BF_4]^-$: (■) 283.15 K, Ref. 41; (●) 293 K, Ref. 54; (▲) 303 K, Ref. 54; (▼) 313 K, Ref. 54; (★) 323.15 K, Ref. 41. (b) $[BMIM]^+[PF_6]^-$: (■) 283.15 K, Ref. 41; (●) 298.15 K, Ref. 41; (▲) 323.15 K, Ref. 41. (c) $[BMIM]^+[Tf_2N]^-$: (■) 279.98 K, Ref. 65; (●) 299.98 K, Ref. 65; (▲) 313.15 K, Ref. 68; (▼) 319.98 K, Ref. 68; (◀) 333.15 K, Ref. 68; (▶) 339.97 K, Ref. 65; (★) 353.15 K, Ref. 68; (□) 373.15 K, Ref. 68; (○) 393.15 K, Ref. 68; (△) 413.15 K, Ref. 68; (▽) 433.15 K, Ref. 68; (☆) 453.15 K, Ref. 68. (d) $[BMPYR]^+[Tf_2N]^-$: (■) 293.10 K, Ref. 75; (●) 333.10 K, Ref. 75; (▲) 373.20 K, Ref. 75; (▼) 413.20 K, Ref. 75. (e) $[BPY]^+[BF_4]^-$: (■) 313.15 K, Ref. 58; (●) 323.15 K, Ref. 58; (▲) 333.15 K, Ref. 58. [Color figure can be viewed in the online issue, which is available at wileyonlinelibrary.com.]

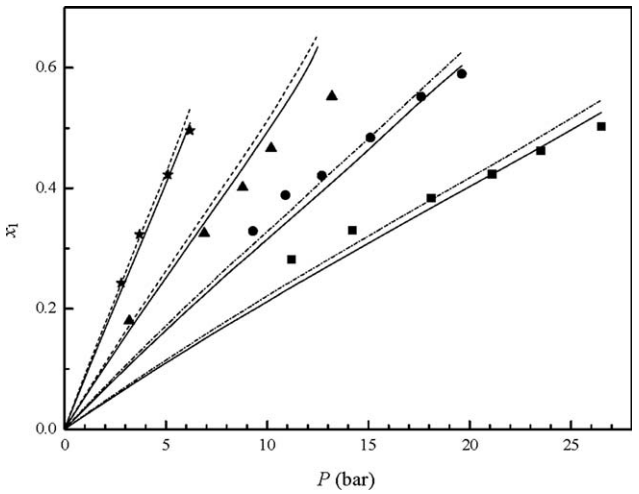

Figure 4. Solubility of CO_2 (1) in $[BMIM]^+[BF_4]^-$ (2) at low temperatures.

Solid lines, predicted results by GCLF EOS with MR1; Dashed lines, predicted results by GCLF EOS with MR2; Scattered points, experimental data. (■) 273.2 K; (●) 258.2 K; (▲) 243.2 K; (★) 228.2 K.

coworkers[106] defined the volume expansivity $\left(\frac{\Delta V}{V}\right)$ of ILs on the basis of molar volume

$$\frac{\Delta V}{V}\% = \frac{\tilde{V}_{\mathrm{M}}(T,P,x) - \tilde{V}_{\mathrm{IL}}(T,P_0)}{\tilde{V}_{\mathrm{IL}}(T,P_0)} \times 100 \qquad (25)$$

where $\tilde{V}_{\mathrm{M}}(T,P,x)$ is the molar volume of IL/CO_2 mixture at a given temperature (T) and pressure (P); and $\tilde{V}_{\mathrm{IL}}(T,P_0)$ is the molar volume of pure IL at the same temperature (T) and ambient pressure ($P_0 = 1$ bar).

The comparison of volume expansivity for 10 kinds of ILs between the predicted results by GCLF EOS (MR1 and MR2) and experimental data collected from references is summarized in Table 3. The molar volumes of pure ILs and IL/CO_2 mixtures, and the corresponding volume expansivity

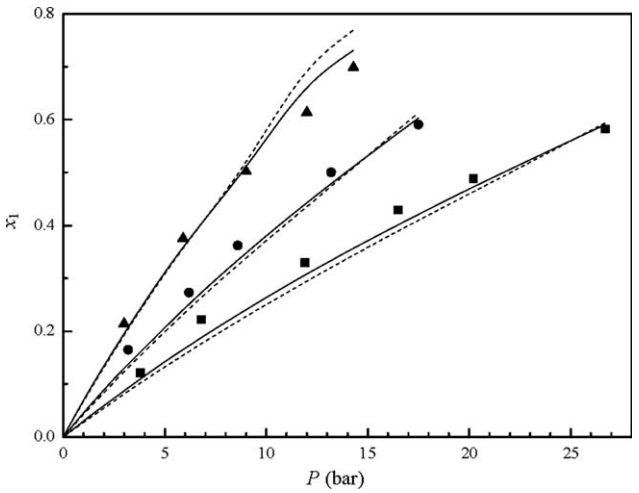

Figure 5. Solubility of CO_2 (1) in $[HMIM]^+[BF_4]^-$ (2) at low temperatures.

Solid lines, predicted results by GCLF EOS with MR1; Dashed lines, predicted results by GCLF EOS with MR2; Scattered points, experimental data. (■) 273.2 K; (●) 258.2 K; (▲) 243.2 K.

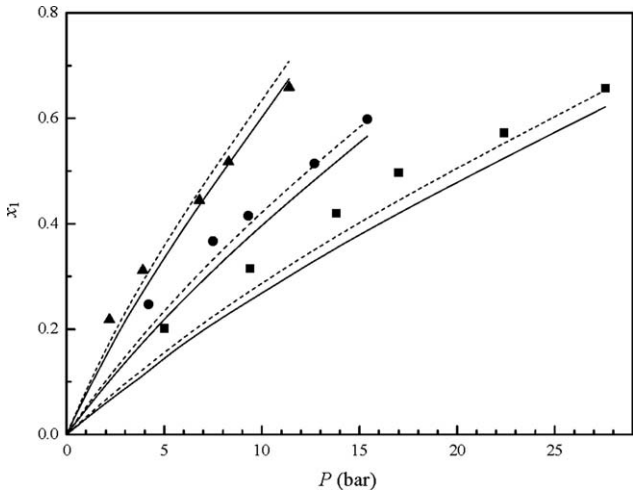

Figure 6. Solubility of CO_2 (1) in $[HMIM]^+[PF_6]^-$ (2) at low temperatures.

Solid lines, predicted results by GCLF EOS with MR1; Dashed lines, predicted results by GCLF EOS with MR2; Scattered points, experimental data. (■) 273.2 K; (●) 258.2 K; (▲) 243.2 K.

are provided in detail in Supporting Information. It can be seen that the predicted results are in good agreement with experimental data, with all the ARDs less than 10%, manifesting the applicability of GCLF EOS for predicting volume expansivity of CO_2–IL systems.

For the imidazolium-based ILs, Aki et al.[40] concluded that volume expansivity was independent on the choice of anions. Herein, we go a further step to explore the influence of different combinations of cations and anions involving 24 kinds of ILs (but not limited to imidazolium-based ILs) and 1261 data points on volume expansivity by using GCLF EOS at temperatures (228–343) K and pressures up to 250 bars. As shown in Figure 7, volume expansivity is almost independent on the kinds of ILs although their molecular weights are quite different. Moreover, there is a linear relationship between the percent volume expansivity $\frac{\Delta V}{V}\%$ and CO_2 solubility in all of the ILs (x)

$$\frac{\Delta V}{V}\% = -89.1950x \qquad (26)$$

with the correlation factor $R^2 = 0.9911$. The larger proportionality constant (-89.195) in comparison with conventional

Table 3. Comparison of Volume Expansivity of ILs upon Addition of CO_2 Between Experimental Data and Predicted Results by GCLF EOS

ILs	MR1 ARD (%)	MR2 ARD (%)	Number of Data Points	References
$[BMIM]^+[BF_4]^-$	5.59	5.56	20	[40]
$[BMIM]^+[TfO]^-$	3.85	3.84	27	[40]
$[BMIM]^+[NO_3]^-$	5.03	5.08	17	[40]
$[BMIM]^+[PF_6]^-$	5.12	5.40	70	[40]
$[BMIM]^+[Tf_2N]^-$	1.60	1.60	59	[40]
$[DMIM]^+[Tf_2N]^-$	4.01	4.00	22	[81]
$[EMIM]^+[Tf_2N]^-$	4.41	4.42	21	[81]
$[HMMIM]^+[Tf_2N]^-$	2.05	1.84	29	[40]
$[HMIM]^+[Tf_2N]^-$	1.31	1.31	28	[40]
$[HMIM]^+[Tf_2N]^-$	9.27	9.26	26	[81]
$[OMIM]^+[Tf_2N]^-$	0.90	0.91	22	[40]

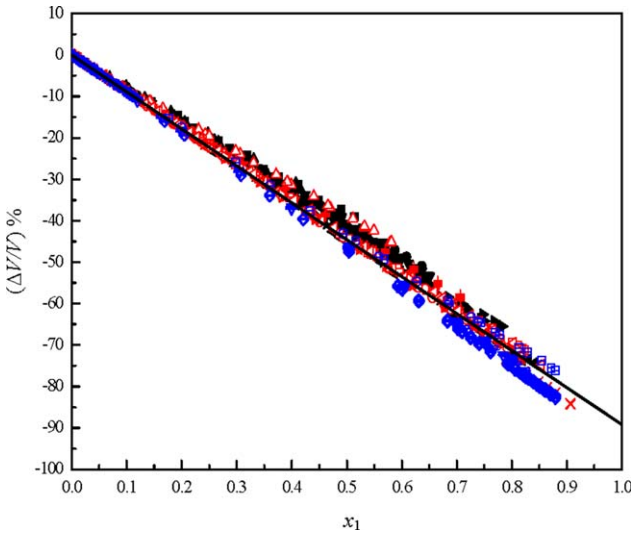

Figure 7. Volume expansivity upon addition of CO_2 (1) for various ILs (2) predicted by GCLF EOS with MR1.

(■) [BMIM][BF_4]; (●) [BMIM][TfO]; (▲) [BMIM][NO_3]; (▼) [BMIM][PF_6]; (◆) [BMIM][Tf_2N]; (◀) [DMIM][Tf_2N]; (▶) [EMIM][Tf_2N]; (★) [HMMIM][Tf_2N]; (□) [HMIM][Tf_2N]; (○) [OMIM][Tf_2N]; (△) [BPY][BF_4]; (▽) [BMPY][Tf_2N]; (◇) [HMPY][Tf_2N]; (◁) [BMPYR][Tf_2N]; (▷) [HMPYR][Tf_2N]; (☆) [OMPYR][Tf_2N]; (+) [BMPYR][TfO]; (×) [$N_{1,8,8,8}$][Tf_2N]; (⊟) [$N_{4,1,1,1}$][Tf_2N]; (⊖) [$N_{2,1,1,3}$][Tf_2N]; (⧋) [$N_{1,4,4,4}$][Tf_2N]; (⧆) [$P_{6,6,6,14}$][Cl]; (⧊) [$P_{6,6,6,14}$][Tf_2N]; (✲) [$P_{1,4,4,4}$][TOS]; Solid lines, linear fitting results. [Color figure can be viewed in the online issue, which is available at wileyonlinelibrary.com.]

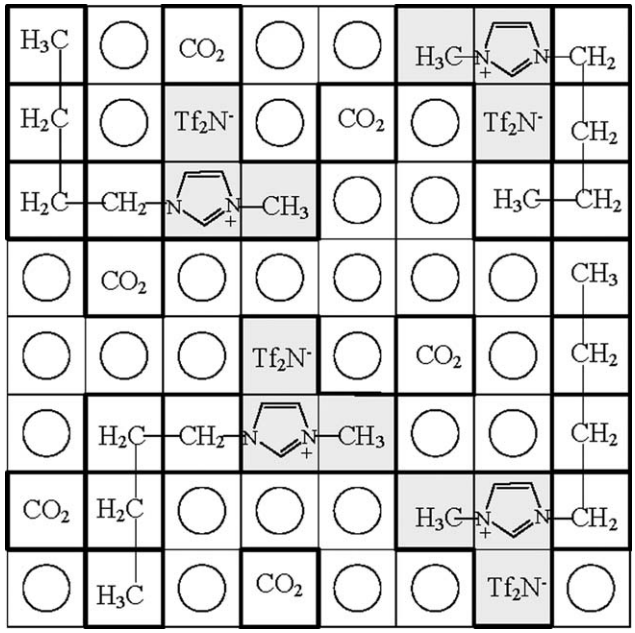

Figure 8. Schematic representation of lattice model for CO_2 molecules, cations, anions, and holes.

organic solvents represents a small volume expansion upon addition of CO_2, indicating that the lattice volume and shape do not change substantially before and after the dissolution of CO_2 in ILs due to the strong electrostatic interaction between cations and anions. Thus, one unique characteristic of ILs is that there is very little volume expansivity upon CO_2 dissolution in the ILs. The solubility difference among ILs will be in some degree attributed to the different fractions of hole volumes (i.e., free volumes) that can be occupied by CO_2 according to the lattice-fluid theory, as illustrated in Figure 8. Therefore, the ILs with long alkyl chain length and weak cation–anion interaction are favorable for increasing CO_2 solubility due to the increased free volume. To the best of our knowledge, this is the first work on predicting and analyzing the volume expansivity by using a predictive thermodynamic model.

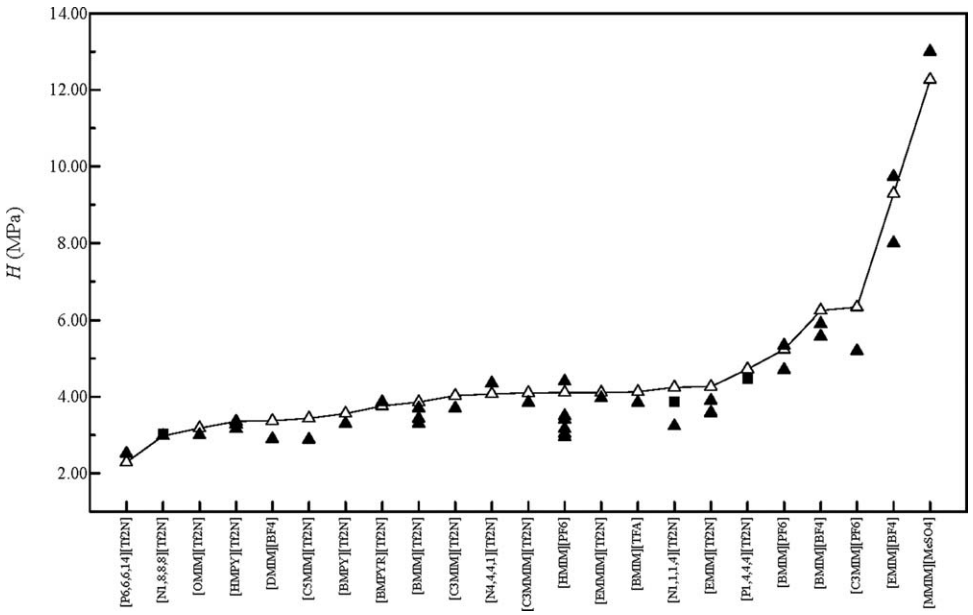

Figure 9. Henry's constants of CO_2 in various ILs at $T = 298.15$ K.

(△) predicted results by GCLF EOS with MR1; (▲) experimental data from references;[38,41,56,64,66,79,95,107–112] (■) experimental data obtained in this work.

Structure–property relation for the solubility of CO_2 in ILs

One of the most important application of predictive models is to identify the structure–property relation between molecular structure of ILs and separation performance (i.e., Henry's constant which reflects the magnitude of CO_2 solubility in various ILs at low pressures) for physical absorption. Based on the mole fraction of CO_2 in CO_2–IL mixture, the Henry's constant can be written as

$$H(T,P)=\lim_{x\to 0}\frac{yP\varphi(T,P)}{x}=\lim_{x\to 0}\gamma P^0(T)=\gamma^{\infty}P^0(T) \qquad (27)$$

where x is mole fraction of CO_2 in the liquid phase (i.e., CO_2 solubility); T and P are the system temperature and pressure, respectively; P^0 is the saturated vapor pressure of CO_2 gas at temperature T, obtained from the Antoine equation using the Antoine constants as proposed by Shiflett and Yokozeki[105]; and γ^{∞} is the activity coefficient of CO_2 in ILs at infinite dilution, calculated by GCLF EOS with MR1 or MR2 mixing rule. Figure 9 shows the Henry's constants of CO_2 in 23 ILs at 298.15 K. It can be seen that the predicted Henry's constants by GCLF EOS (MR1) exhibit the similar trend as the experimental values collected from references.[38,41,56,64,66,79,95,107–112]

In order to achieve a deep insight into structure–property relation, we measured the solubility of CO_2 in $[N_{1,8,8,8}]^+[Tf_2N]^-$, $[N_{1,4,4,4}]^+[Tf_2N]^-$, and $[P_{1,4,4,4}]^+[Tf_2N]^-$ at 298.2 K and pressures up to 8.0 bar in this work, and the solubility data are listed in Supporting Information. The corresponding Henry's constants are deduced from the linear extrapolation of experimental CO_2 solubility in ILs. As shown in Figure 9, for the ILs with the same anion $[Tf_2N]^-$, the difference of Henry's constants among imidazolium, pyrrolidinium, and pyridinium-based cations is not significant with n (the number of carbon atoms in the alkyl chain on cation of ILs) < 8. However, for the ILs with ammonium and phosphonium-based cations and the same anion $[Tf_2N]^-$, the Henry's constants follow the order of $[P_{6,6,6,14}]^+ < [N_{1,8,8,8}]^+ < [N_{4,4,4,1}]^+ < [N_{1,1,1,4}]^+ < [P_{1,4,4,4}]^+$, and the maximum value with $n < 8$ is twice as much as the minimum value with $n >> 8$. Similarly, for the ILs with imidazolium-based cations and the same anion $[BF_4]^-$, the maximum Henry's constant for $[EMIM]^+[BF_4]^-$ is triplicate as much as the minimum one for $[DMIM]^+[BF_4]^-$. Moreover, for most of the investigated ILs with the anion $[Tf_2N]^-$, their Henry's constants are indeed higher than that for $[DMIM]^+[BF_4]^-$. Therefore, the long alkyl chain length on the cation may influence CO_2 solubility effectively. Care should be taken to consider the cation effect, although some authors claimed that the primary contribution to gas solubility is anion effect.[53,113,114]

Conclusions

The application of GCLF EOS with two mixing rules, i.e., MR1 and MR2, has been extended to the important CO_2–IL systems, and 22 new group binary interaction parameters α_{mn} between CO_2 and IL groups were added into the current GCLF EOS parameter matrix so that it may become a universal and available equation of state for conventional organic solvents, polymers, ILs, and gas molecules. From this work, the following conclusions can be drawn: (1) GCLF EOS can be used for predicting the CO_2 solubility in ILs at either high (above 278.15 K) or low temperatures (below 278.15 K), although the group binary interaction parameters were derived from the experimental solubility data at high temperatures. To the best of our knowledge, this should be the first work that presents the solubility data of CO_2 in ILs at low temperatures (below 278.15 K). (2) The volume expansivity is independent on the different combinations of cations and anions, and exhibits a linear relationship with CO_2 solubility as defined in Eq. 26 over a wide temperature and pressure range. (3) The influence of alkyl chain length on the cation on CO_2 solubility cannot be underestimated in some cases. With the same anion, there is a minor difference in Henry's constants for ILs with a short alkyl chain length on the cation. But when the alkyl chain length increases to a certain degree, the Henry's constant will decrease significantly because the free volume effect becomes effective. Anyway, this work confirms the strong predictive power of GCLF EOS for CO_2–IL systems.

Acknowledgment

This work was financially supported by the National Nature Science Foundation of China under Grants (Nos. 21121064 and 21076008).

Literature Cited

1. Brennecke JF, Maginn EJ. Ionic liquids: Innovative fluids for chemical processing. *AIChE J*. 2001;47:2384–2389.
2. Earle MJ, Esperanca JMSS, Gilea MA, Canongia Lopes JN, Rebelo LPN, Magee JW, Seddon KR, Widegren JA. The distillation and volatility of ionic liquids. *Nature*. 2006;439:831–834.
3. Lurgi GmbH. Available at: http://uicgroupecho.wikispaces.com/file/view/B_0308e_Rectisol.pdf. Accessed June 15, 2013.
4. Lei Z, Chen B, Li C, Liu H. Predictive molecular thermodynamic models for liquid solvents, solid salts, polymers, and ionic liquids. *Chem Rev*. 2008;108:1419–1455.
5. Kilaru PK, Condemarin RA, Scovazzo P. Correlations of low-pressure carbon dioxide and hydrocarbon solubilities in imidazolium-, phosphonium-, and ammonium-based room-temperature ionic liquids. Part 1. Using surface tension. *Ind Eng Chem Res*. 2008;47:900–909.
6. Kilaru PK, Scovazzo P. Correlations of low-pressure carbon dioxide and hydrocarbon solubilities in imidazolium-, phosphonium-, and ammonium-based room-temperature ionic liquids. Part 2. Using activation energy of viscosity. *Ind Eng Chem Res*. 2008;47:910–919.
7. Bara JE, Carlisle TK, Gabriel CJ, Camper D, Finotello A, Gin DL, Noble RD. Guide to CO_2 separations in imidazolium-based room-temperature ionic liquids. *Ind Eng Chem Res*. 2009;48:2739–2751.
8. Camper D, Becker C, Koval C, Noble R. Low pressure hydrocarbon solubility in room temperature ionic liquids containing imidazolium rings interpreted using regular solution theory. *Ind Eng Chem Res*. 2005;44:1928–1933.
9. Kato R, Gmehling J. Measurement and correlation of vapor-liquid equilibria of binary systems containing the ionic liquids [EMIM][$(CF_3SO_2)_2N$], [BMIM][$(CF_3SO_2)_2N$], [MMIM][$(CH_3)_2PO_4$] and oxygenated organic compounds respectively water. *Fluid Phase Equilib*. 2005;231:38–43.
10. Nebig S, Liebert V, Gmehling J. Measurement and prediction of activity coefficients at infinite dilution (γ^{∞}), vapor–liquid equilibria (VLE) and excess enthalpies (H^E) of binary systems with 1,1-dialkyl-pyrrolidinium bis(trifluoromethylsulfonyl)imide using mod. UNIFAC (Dortmund). *Fluid Phase Equilib*. 2009;277:61–67.
11. Nebig S, Gmehling J. Prediction of phase equilibria and excess properties for systems with ionic liquids using modified UNIFAC: Typical results and present status of the modified UNIFAC matrix for ionic liquids. *Fluid Phase Equilib*. 2011;302:220–225.
12. Diedenhofen M, Eckert F, Klamt A. Prediction of infinite dilution activity coefficients of organic compounds in ionic liquids using COSMO-RS. *J Chem Eng Data*. 2003;48:475–479.

13. Manan NA, Hardacre C, Jacquemin J, Rooney DW, Youngs TGA. Evaluation of gas solubility prediction in ionic liquids using COSMOthermX. *J Chem Eng Data*. 2009;54:2005–2022.
14. Diedenhofen M, Klamt A. COSMO-RS as a tool for property prediction of IL mixtures – A review. *Fluid Phase Equilib*. 2010;294:31–38.
15. Lei Z, Chen B, Li C. COSMO-RS modeling on the extraction of stimulant drugs from urine sample by the double actions of supercritical carbon dioxide and ionic liquid. *Chem Eng Sci*. 2007;62:3940–3950.
16. Kim YS, Choi WY, Jang JH, Yoo KP, Lee CS. Solubility measurement and prediction of carbon dioxide in ionic liquids. *Fluid Phase Equilib*. 2005;228-229:439–445.
17. Kim JE, Lim JS, Kang JW. Measurement and correlation of solubility of carbon dioxide in 1-alkyl-3-methylimidazolium hexafluorophosphate ionic liquids. *Fluid Phase Equilib*. 2011;306:251–255.
18. Paduszyński K, Chiyen J, Ramjugernath D, Letcher TM, Domańska U. Liquid-liquid phase equilibrium of (piperidinium-based ionic liquid + an alcohol) binary systems and modelling with NRHB and PCP-SAFT. *Fluid Phase Equilib*. 2011;305:43–52.
19. Paduszyński K, Domańska U. Solubility of aliphatic hydrocarbons in piperidinium ionic liquids: Measurements and modeling in terms of perturbed-chain statistical associating fluid theory and nonrandom hydrogen-bonding theory. *J Phy Chem B*. 2011;115:12537–12548.
20. Vega LF, Vilaseca O, Llovell F, Andreu JS. Modeling ionic liquids and the solubility of gases in them: Recent advances and perspectives. *Fluid Phase Equilib*. 2010;294:15–30.
21. Vega LF, Jackson G. 20 years of the SAFT equation of state – Recent advances and challenges symposium held in Bellaterra, Barcelona, 19–21 September 2010. *Fluid Phase Equilib*. 2011;306:1–3.
22. Ji X, Adidharma H. Thermodynamic modeling of CO_2 solubility in ionic liquid with heterosegmented statistical associating fluid theory. *Fluid Phase Equilib*. 2010;293:141–150.
23. Ji X, Adidharma H. Prediction of molar volume and partial molar volume for CO_2/ionic liquid systems with heterosegmented statistical associating fluid theory. *Fluid Phase Equilib*. 2012;315:53–63.
24. Ashrafmansouri SS, Raeissi S. Modeling gas solubility in ionic liquids with the SAFT-γ group contribution method. *J Supercrit Fluids*. 2012;63:81–91.
25. Andreu JS, Vega LF. Capturing the solubility behavior of CO_2 in ionic liquids by a simple model. *J Phys Chem C*. 2007;111:16028–16034.
26. Andreu JS, Vega LF. Modeling the solubility behavior of CO_2, H_2, and Xe in [C_n-mim][Tf_2N] ionic liquids. *J Phys Chem B*. 2008;112:15398–15406.
27. Ji X, Held C, Sadowski G. Modeling imidazolium-based ionic liquids with ePC-SAFT. *Fluid Phase Equilib*. 2012;335:64–73.
28. Rahmati-Rostami M, Behzadi B, Ghotbi C. Thermodynamic modeling of hydrogen sulfide solubility in ionic liquids using modified SAFT-VR and PC-SAFT equations of state. *Fluid Phase Equilib*. 2011;309:179–189.
29. Bermejo MD, Martin A, Foco G, Cocero MJ, Bottini SB, Peters CJ. Application of a group contribution equation of state for the thermodynamic modeling of the binary systems CO_2−1-butyl-3-methyl imidazolium nitrate and CO_2−1-hydroxy-1-propyl-3-methyl imidazolium nitrate. *J Supercrit Fluids*. 2009;50:112–117.
30. Karakatsani EK, Economou IG, Kroon MC, Peters CJ, Witkamp GJ. tPC-PSAFT modeling of gas solubility in imidazolium-based ionic liquids. *J Phys Chem C*. 2007;111:15487–15492.
31. High MS, Danner RP. A group contribution equation of state for polymer solutions. *Fluid Phase Equilib*. 1989;53:323–330.
32. High MS, Danner RP. Application of the group contribution lattice-fluid EOS to polymer solutions. *AIChE J*. 1990;36:1625–1632.
33. Lee BC, Danner RP. Application of the group-contribution lattice-fluid equation of state to random copolymer-solvent systems. *Fluid Phase Equilib*. 1996;117:33–39.
34. Li J, Lei Z, Chen B, Li C. Extension of the group-contribution lattice-fluid equation of state. *Fluid Phase Equilib*. 2007;260:135–145.
35. Hamedi M, Muralidharan V, Lee BC, Danner RP. Prediction of carbon dioxide solubility in polymers based on a group-contribution equation of state. *Fluid Phase Equilib*. 2003;204:41–53.
36. Lei Z, Xiao L, Dai C, Chen B. Group contribution lattice fluid equation of state (GCLF EOS) for ionic liquids. *Chem Eng Sci*. 2012;75:1–13.
37. Blanchard LA, Hancu D, Beckman EJ, Brennecke JF. Green processing using ionic liquids and CO_2. *Nature*. 1999;399:28–29.
38. Lei Z, Yuan J, Zhu J. Solubility of CO_2 in propanone, 1-ethyl-3-methylimidazolium tetrafluoroborate, and their mixtures. *J Chem Eng Data*. 2010;55:4190–4194.
39. Shiflett MB, Yokozeki A. Solubilities and diffusivities of carbon dioxide in ionic liquids: [bmim][PF_6] and [bmim][BF_4]. *Ind Eng Chem Res*. 2005;44:4453–4464.
40. Aki SNVK, Mellein BR, Saurer EM, Brennecke JF. High-pressure phase behavior of carbon dioxide with imidazolium-based ionic liquids. *J Phys Chem B*. 2004;108:20355–20365.
41. Anthony JL, Anderson JL, Maginn EJ, Brennecke JF. Anion effects on gas solubility in ionic liquids. *J Phys Chem B*. 2005;109:6366–6374.
42. Yokozeki A, Shiflett MB, Junk CP, Grieco LM, Foo T. Physical and chemical absorptions of carbon dioxide in room-temperature ionic liquids. *J Phys Chem B*. 2008;112:16654–16663.
43. Tian S, Hou Y, Wu W, Ren S, Pang K. Physical properties of 1-butyl-3-methylimidazolium tetrafluoroborate/*N*-methyl-2-pyrrolidone mixtures and the solubility of CO_2 in the system at elevated pressures. *J Chem Eng Data*. 2012;57:756–763.
44. Lei Z, Zhang J, Li Q, Chen B. UNIFAC model for ionic liquids. *Ind Eng Chem Res*. 2009;48:2697–2704.
45. Alevizou EI, Pappa GD, Voutsas EC. Prediction of phase equilibrium in mixtures containing ionic liquids using UNIFAC. *Fluid Phase Equilib*. 2009;284:99–105.
46. Valderrama JO, Zarricueta K. A simple and generalized model for predicting the density of ionic liquids. *Fluid Phase Equilib*. 2009;275:145–151.
47. Lee BC, Danner RP. Prediction of polymer-solvent phase equilibria by a modified group-contribution EOS. *AIChE J*. 1996;42:837–849.
48. Danner RP, Hamedi M, Lee BC. Applications of the group-contribution, lattice-fluid equation of state. *Fluid Phase Equilib*. 2002;194-197:619–639.
49. Jones AT, Zielinski JM, Danner RP. Solubility predictions for copolymer systems. *Fluid Phase Equilib*. 2009;280:88–93.
50. Husson-Borg P, Majer V, Costa Gomes MF. Solubilities of oxygen and carbon dioxide in butyl methyl imidazolium tetrafluoroborate as a function of temperature and at pressures close to atmospheric pressure. *J Chem Eng Data*. 2003;48: 480–485.
51. Kroon MC, Shariati A, Costantini M, van Spronsen J, Witkamp GJ, Sheldon RA, Peters CJ. High-pressure phase behavior of systems with ionic liquids: Part V. The binary system carbon dioxide + 1-butyl-3-methylimidazolium tetrafluoroborate. *J Chem Eng Data*. 2005;50:173–176.
52. Jacquemin J, Costa Gomes MF, Husson P, Majer V. Solubility of carbon dioxide, ethane, methane, oxygen, nitrogen, hydrogen, argon, and carbon monoxide in 1-butyl-3-methylimidazolium tetrafluoroborate between temperatures 283 K and 343 K and at pressures close to atmospheric. *J Chem Thermodyn*. 2006;38:490–502.
53. Chen Y, Zhang S, Yuan X, Zhang Y, Zhang X, Dai W, Mori R. Solubility of CO_2 in imidazolium-based tetrafluoroborate ionic liquids. *Thermochim Acta*. 2006;441:42–44.
54. Revelli AL, Mutelet F, Jaubert JN. High carbon dioxide solubilities in imidazolium-based ionic liquids and in poly(ethylene glycol) dimethyl ether. *J Phys Chem B*. 2010;114:12908–12913.
55. Jang S, Cho DW, Im T, Kim H. High-pressure phase behavior of CO_2 + 1-butyl-3-methylimidazolium chloride system. *Fluid Phase Equilib*. 2010;299:216–221.
56. Muldoon MJ, Aki SNVK, Anderson JL, Dixon JK, Brennecke JF. Improving carbon dioxide solubility in ionic liquids. *J Phys Chem B*. 2007;111:9001–9009.
57. Kumełan J, Tuma D, Maurer G. Solubility of CO_2 in the ionic liquids [bmim][CH_3SO_4] and [bmim][PF_6]. *J Chem Eng Data*. 2006;51:1802–1807.
58. Blanchard LA, Gu Z, Brennecke JF. High-pressure phase behavior of ionic liquid/CO_2 systems. *J Phys Chem B*. 2001;105:2437–2444.
59. Bermejo MD, Montero M, Saez E, Florusse LJ, Kotlewska AJ, Cocero MJ, van Rantwijk F, Peters CJ. Liquid-vapor equilibrium of the systems butylmethylimidazolium nitrate-CO_2 and hydroxypropylmethylimidazolium nitrate-CO_2 at high pressure: Influence of water on the phase behavior. *J Phys Chem B*. 2008;112:13532–13541.
60. Anthony JL, Maginn EJ, Brennecke JF. Solubilities and thermodynamic properties of gases in the ionic liquid 1-*n*-butyl-3-methylimidazolium hexafluorophosphate. *J Phys Chem B*. 2002;106:7315–7320.
61. Pérez-Salado Kamps Á, Tuma D, Xia J, Maurer G. Solubility of CO_2 in the ionic liquid [bmim][PF_6]. *J Chem Eng Data*. 2003;48:746–749.

62. Shariati A, Gutkowski K, Peters CJ. Comparison of the phase behavior of some selected binary systems with ionic liquids. *AIChE J*. 2005;51:1532–1540.
63. Zhang S, Yuan X, Chen Y, Zhang X. Solubilities of CO_2 in 1-butyl-3-methylimidazolium hexafluorophosphate and 1,1,3,3-tetramethylguanidium lactate at elevated pressures. *J Chem Eng Data*. 2005;50:1582–1585.
64. Jacquemin J, Husson P, Majer V, Gomes MFC. Low-pressure solubilities and thermodynamics of solvation of eight gases in 1-butyl-3-methylimidazolium hexafluorophosphate. *Fluid Phase Equilib*. 2006;240:87–95.
65. Lee BC, Outcalt SL. Solubilities of gases in the ionic liquid 1-*n*-butyl-3-methylimidazolium bis(trifluoromethylsulfonyl)imide. *J Chem Eng Data*. 2006;51:892–897.
66. Jacquemin J, Husson P, Majer V, Costa Gomes M. Influence of the cation on the solubility of CO_2 and H_2 in ionic liquids based on the bis(trifluoromethylsulfonyl)imide anion. *J Solution Chem*. 2007;36:967–979.
67. Shin EK, Lee BC, Lim JS. High-pressure solubilities of carbon dioxide in ionic liquids: 1-alkyl-3-methylimidazolium bis(trifluoromethylsulfonyl)imide. *J Supercrit Fluids*. 2008;45:282–292.
68. Raeissi S, Peters CJ. Carbon dioxide solubility in the homologous 1-alkyl-3-methylimidazolium bis(trifluoromethylsulfonyl)imide family. *J Chem Eng Data*. 2009;54:382–386.
69. Carvalho PJ, Álvarez VH, Marrucho IM, Aznar M, Coutinho JAP. High pressure phase behavior of carbon dioxide in 1-butyl-3-methylimidazolium bis(trifluoromethylsulfonyl)imide and 1-butyl-3-methylimidazolium dicyanamide ionic liquids. *J Supercrit Fluids*. 2009;50:105–111.
70. Manic MS, Queimada AJ, Macedo EA, Najdanovic-Visak V. High-pressure solubilities of carbon dioxide in ionic liquids based on bis(trifluoromethylsulfonyl)imide and chloride. *J Supercrit Fluids*. 2012;65:1–10.
71. Carvalho PJ, Alvarez VH, Schroöder B, Gil AM, Marrucho IM, Aznar M, Santos LMNBF, Coutinho JAP. Specific solvation interactions of CO_2 on acetate and trifluoroacetate imidazolium based ionic liquids at high pressures. *J Phys Chem B*. 2009;113:6803–6812.
72. Shin EK, Lee BC. High-pressure phase behavior of carbon dioxide with ionic liquids: 1-alkyl-3-methylimidazolium trifluoromethanesulfonate. *J Chem Eng Data*. 2008;53:2728–2734.
73. Soriano AN, Doma Jr. BT, Li MH. Carbon dioxide solubility in some ionic liquids at moderate pressures. *J Taiwan Inst Chem Eng*. 2009;40:387–393.
74. Hong G, Jacquemin J, Deetlefs M, Hardacre C, Husson P, Costa Gomes MF. Solubility of carbon dioxide and ethane in three ionic liquids based on the bis{(trifluoromethyl)sulfonyl}imide anion. *Fluid Phase Equilib*. 2007;257:27–34.
75. Kumełan J, Tuma D, Pérez-Salado Kamps Á, Maurer G. Solubility of the single gases carbon dioxide and hydrogen in the ionic liquid [bmpy][Tf_2N]. *J Chem Eng Data*. 2010;55:165–172.
76. Yim JH, Song HN, Yoo KP, Lim JS. Measurement of CO_2 solubility in ionic liquids: [BMP][Tf_2N] and [BMP][$MeSO_4$] by measuring bubble-point pressure. *J Chem Eng Data*. 2011;56:1197–1203.
77. Song HN, Lee B-C, Lim JS. Measurement of CO_2 Solubility in ionic liquids: [BMP][TfO] and [$P_{14,6,6,6}$][Tf_2N] by measuring bubble-point pressure. *J Chem Eng Data*. 2009;55:891–896.
78. Sharma P, Choi SH, Park SD, Baek IH, Lee GS. Selective chemical separation of carbondioxide by ether functionalized imidazolium cation based ionic liquids. *Chem Eng J*. 2012;181–182:834–841.
79. Carvalho PJ, Álvarez VH, Machado JJB, Pauly J, Daridon JL, Marrucho IM, Aznar M, Coutinho JAP. High pressure phase behavior of carbon dioxide in 1-alkyl-3-methylimidazolium bis(trifluoromethylsulfonyl)imide ionic liquids. *J Supercrit Fluids*. 2009;48:99–107.
80. Ren W. *High-pressure phase equilibria of ionic liquids and compressed gases for applications in reactions and absorption refrigeration* [Ph. D. Thesis]. Kansas, USA: University of Kansas, 2009.
81. Ren W, Sensenich B, Scurto AM. High-pressure phase equilibria of {carbon dioxide (CO_2) + *n*-alkyl-imidazolium bis(trifluoromethylsulfonyl)amide} ionic liquids. *J Chem Thermodyn*. 2010;42:305–311.
82. Bogel-Łukasik R, Matkowska D, Bogel-Łukasik E, Hofman T. Isothermal vapour-liquid equilibria in the binary and ternary systems consisting of an ionic liquid, 1-propanol and CO_2. *Fluid Phase Equilib*. 2010;293:168–174.
83. Soriano AN, Doma BT, Li MH. Solubility of carbon dioxide in 1-ethyl-3-methylimidazolium tetrafluoroborate. *J Chem Eng Data*. 2008;53:2550–2555.
84. Palgunadi J, Kang JE, Nguyen DQ, Kim JH, Min BK, Lee SD, Kim H, Kim HS. Solubility of CO_2 in dialkylimidazolium dialkylphosphate ionic liquids. *Thermochim Acta*. 2009;494:94–98.
85. Jalili AH, Mehdizadeh A, Shokouhi M, Ahmadi AN, Hosseini-Jenab M, Fateminassab F. Solubility and diffusion of CO_2 and H_2S in the ionic liquid 1-ethyl-3-methylimidazolium ethylsulfate. *J Chem Thermodyn*. 2010;42:1298–1303.
86. Soriano AN, Doma Jr. BT, Li MH. Solubility of carbon dioxide in 1-ethyl-3-methylimidazolium 2-(2-methoxyethoxy) ethylsulfate. *J Chem Thermodyn*. 2008;40:1654–1660.
87. Shariati A, Peters CJ. High-pressure phase behavior of systems with ionic liquids: II. The binary system carbon dioxide + 1-ethyl-3-methylimidazolium hexafluorophosphate. *J Supercrit Fluids*. 2004;29:43–48.
88. Hong G, Jacquemin J, Husson P, Costa Gomes MF, Deetlefs M, Nieuwenhuyzen M, Sheppard O, Hardacre C. Effect of acetonitrile on the solubility of carbon dioxide in 1-ethyl-3-methylimidazolium bis(trifluoromethylsulfonyl)amide. *Ind Eng Chem Res*. 2006;45:8180–8188.
89. Schilderman AM, Raeissi S, Peters CJ. Solubility of carbon dioxide in the ionic liquid 1-ethyl-3-methylimidazolium bis(trifluoromethylsulfonyl)imide. *Fluid Phase Equilib*. 2007;260:19–22.
90. Shiflett MB, Yokozeki A. Phase behavior of carbon dioxide in ionic liquids: [emim][acetate], [emim][trifluoroacetate], and [emim][acetate] + [emim][trifluoroacetate] mixtures. *J Chem Eng Data*. 2009;54:108–114.
91. Soriano AN, Doma Jr. BT, Li MH. Carbon dioxide solubility in 1-ethyl-3-methylimidazolium trifluoromethanesulfonate. *J Chem Thermodyn*. 2009;41:525–529.
92. Costantini M, Toussaint VA, Shariati A, Peters CJ, Kikic I. High-pressure phase behavior of systems with ionic liquids: Part iv. Binary system carbon dioxide + 1-hexyl-3-methylimidazolium tetrafluoroborate. *J Chem Eng Data*. 2005;50:52–55.
93. Shariati A, Peters CJ. High-pressure phase behavior of systems with ionic liquids: Part III. The binary system carbon dioxide + 1-hexyl-3-methylimidazolium hexafluorophosphate. *J Supercrit Fluids*. 2004;30:139–144.
94. Kumełan J, Pérez-Salado Kamps Á, Tuma D, Maurer G. Solubility of CO_2 in the ionic liquid [hmim][Tf_2N]. *J Chem Thermodyn*. 2006;38:1396–1401.
95. Costa Gomes MF. Low-pressure solubility and thermodynamics of solvation of carbon dioxide, ethane, and hydrogen in 1-hexyl-3-methylimidazolium bis(trifluoromethylsulfonyl)amide between temperatures of 283 K and 343 K. *J Chem Eng Data*. 2007;52:472–475.
96. Shiflett MB, Yokozeki A. Solubility of CO_2 in room temperature ionic liquid [hmim][Tf_2N]. *J Phys Chem B*. 2007;111:2070–2074.
97. Kim YS, Jang JH, Lim BD, Kang JW, Lee CS. Solubility of mixed gases containing carbon dioxide in ionic liquids: Measurements and predictions. *Fluid Phase Equilib*. 2007;256:70–74.
98. Raeissi S, Florusse L, Peters CJ. Scott-van konynenburg phase diagram of carbon dioxide + alkylimidazolium-based ionic liquids. *J Supercrit Fluids*. 2010;55:825–832.
99. Mellein BR, Brennecke JF. Characterization of the ability of CO_2 to act as an antisolvent for ionic liquid/organic mixtures. *J Phys Chem B*. 2007;111:4837–4843.
100. Yim JH, Song HN, Lee BC, Lim JS. High-pressure phase behavior of binary mixtures containing ionic liquid [HMP][Tf_2N], [OMP][Tf_2N] and carbon dioxide. *Fluid Phase Equilib*. 2011;308:147–152.
101. Gutkowski KI, Shariati A, Peters CJ. High-pressure phase behavior of the binary ionic liquid system 1-octyl-3-methylimidazolium tetrafluoroborate + carbon dioxide. *J Supercrit Fluids*. 2006;39:187–191.
102. Jalili AH, Safavi M, Ghotbi C, Mehdizadeh A, Hosseini-Jenab M, Taghikhani V. Solubility of CO_2, H_2S, and their mixture in the ionic liquid 1-octyl-3-methylimidazolium bis(trifluoromethyl)sulfonylimide. *J Phys Chem B*. 2012;116:2758–2774.
103. Carvalhoa PJ, Álvarezb VH, Marruchoa IM, Aznarb M, Coutinho JAP. High carbon dioxide solubilities in trihexyltetradecylphosphonium-based ionic liquids. *J Supercrit Fluids*. 2010;52:258–265.
104. Scientific Computing & Modeling. Available at: http://www.scm.com/Doc/Doc2010/CRS/CRS/page18.html. Accessed June 15, 2013.
105. Shiflett MB, Yokozeki A. Solubility and diffusivity of hydrofluorocarbons in room-temperature ionic liquids. *AIChE J*. 2006;52:1205–1219.

106. de la Fuente Badilla JC, Peters CJ, de Swaan Arons J. Volume expansion in relation to the gas-antisolvent process. *J Supercrit Fluids*. 2000;17:13–23.
107. Baltus RE, Culbertson BH, Dai S, Luo H, DePaoli DW. Low-pressure solubility of carbon dioxide in room-temperature ionic liquids measured with a quartz crystal microbalance. *J Phys Chem B*. 2004;108:721–727.
108. Anderson JL, Dixon JK, Maginn EJ, Brennecke JF. Measurement of SO_2 solubility in ionic liquids. *J Phys Chem B*. 2006;110:15059–15062.
109. Camper D, Bara J, Koval C, Noble R. Bulk-fluid solubility and membrane feasibility of Rmim-based room-temperature ionic liquids. *Ind Eng Chem Res*. 2006;45:6279–6283.
110. Hou Y, Baltus RE. Experimental measurement of the solubility and diffusivity of CO_2 in room-temperature ionic liquids using a transient thin-liquid-film method. *Ind Eng Chem Res*. 2007;46:8166–8175.
111. Finotello A, Bara JE, Camper D, Noble RD. Room-temperature ionic liquids: Temperature dependence of gas solubility selectivity. *Ind Eng Chem Res*. 2008;47:3453–3459.
112. Urukova I, Vorholz J, Maurer G. Solubility of CO_2, CO, and H_2 in the ionic liquid [bmim][PF_6] from Monte Carlo simulations. *J Phys Chem B*. 2005;109:12154–12159.
113. Hu YF, Liu ZC, Xu CM, Zhang XM. The molecular characteristics dominating the solubility of gases in ionic liquids. *Chem Soc Rev*. 2011;40:3802–3823.
114. Anderson JL, Dixon JK, Brennecke JF. Solubility of CO_2, CH_4, C_2H_6, C_2H_4, O_2, and N_2 in 1-hexyl-3-methylpyridinium bis(trifluoromethylsulfonyl)imide: Comparison to other ionic liquids. *Acc Chem Res*. 2007;40:1208–1216.

Manuscript received Sept. 13, 2012, and revision received Apr. 25, 2013.